


# Bulk Fermi arc transition induced large photogalvanic effect in Weyl semimetals

Jin Cao,<sup>\*</sup> Maoyuan Wang<sup>✉,\*</sup>, Zhi-Ming Yu<sup>✉,†</sup>, and Yugui Yao<sup>‡</sup>

*Centre for Quantum Physics, Key Laboratory of Advanced Optoelectronic Quantum Architecture and Measurement (MOE),  
School of Physics, Beijing Institute of Technology, Beijing 100081, China  
and Beijing Key Lab of Nanophotonics & Ultrafine Optoelectronic Systems, School of Physics,  
Beijing Institute of Technology, Beijing 100081, China*

 (Received 23 August 2021; revised 31 August 2022; accepted 8 September 2022; published 19 September 2022)

The surface Fermi arc, as a hallmark of Weyl semimetals (WSMs), has been well known in current research, but it remains a challenge to unveil novel phenomena associated with the Fermi arc. Here, in WSMs, namely, the photoinduced transition between the bulk states and the Fermi arc. We find this process is significant and can lead to a large effective three-dimensional shift current on the boundaries with the Fermi arc in wide terahertz range. Moreover, due to the low symmetry of the boundaries, the surface photogalvanic effect predicted here can appear in a large class of WSMs that can not have bulk shift current. Hence, our work not only unveils a hidden photogalvanic effect in WSMs but also suggests that all the WSMs are promising material candidates for developing efficient terahertz photodetectors.

DOI: [10.1103/PhysRevB.106.125416](https://doi.org/10.1103/PhysRevB.106.125416)

## I. INTRODUCTION

The photogalvanic effect refers to the generation of dc electric current in a material illuminated by light [1]. It has been attracting intensive interest in condensed matter physics, due to the promising application on photodetectors and solar cells beyond pn junction structure [2–12]. In addition to technological application, the photogalvanic effect also provides a basic mechanism to probe various geometric quantities of systems, such as Berry curvature, quantum metric, and Christoffel symbols [13–21,21,22].

Generally, the dominant dc response of materials under a monochromatic light characterized by  $A(t) = A(\omega)e^{-i\omega t} + \text{c.c.}$  is quadratic. As a representative photogalvanic effect, the linear shift current can be expressed as [13,23]

$$j^a = \sigma_{bc}^a(\omega)E^b(\omega)E^c(-\omega), \quad (1)$$

with  $\sigma_{bc}^a$  the third-rank shift conductivity tensor and  $\mathbf{E}(\omega) = i\omega\mathbf{A}(\omega)$ . Here, we have adopted the Einstein summation convention and the letters  $a, b, \dots$  denote Cartesian indexes. Clearly, the tensor  $\sigma_{bc}^a$  is constrained by the (magnetic) point group of the systems. For example, when the system has spatial inversion symmetry  $\mathcal{P}$ ,  $\sigma_{bc}^a$  should vanish, as both  $\mathbf{j}$  and  $\mathbf{E}$  change sign under  $\mathcal{P}$ . Hence, the studies of shift current effect generally focus on noncentrosymmetric materials [24,25].

Many efforts have been devoted to searching for material candidates with significant shift current effect [26]. For example, Cook *et al.* [27] and Rangel *et al.* [28] showed that the semiconductors with semi-Dirac-type dispersion like single-layer monochalcogenides can exhibit large shift cur-

rent, which is comparable to conventional solar cells based on pn junction.

Currently, the study has been focusing on topological WSMs [29–43]. In WSMs, the conduction band and the valence band form Weyl points in the bulk, around which all the geometric quantities become divergent [44]. Hence, the WSMs are expected to exhibit large shift current in low-energy frequency and then are considered as promising materials for designing terahertz photodetectors [25]. However, to generate large shift current in bulk, one has to break  $\mathcal{P}$  symmetry, tilt the Weyl spectra, and tune the Fermi level near Weyl points [32]. Consequently, a large class of WSMs, such as centrosymmetric WSMs and Kramers-WSMs [45,46] are forbidden by symmetries to have net bulk shift current. This poses outstanding restrictions for the exploration of terahertz photodetectors.

Surface Fermi arc state is another interesting property of topological WSMs [47,48]. A few previous works also studied the surface photogalvanic effect in the WSMs [49–51]. However, the photogalvanic effect there are negligible in terahertz range.

In this work, we show that large surface shift current can be generated in terahertz range by process, namely, the photoinduced transition between bulk states and the surface Fermi arc in WSMs, termed as bulk-Fermi-arc transition here. A key observation is that the surface Fermi arc is always attached to bulk Weyl cones [47], indicating a gapless feature of the Fermi arc. Moreover, there exists sizable overlap between the bulk states and the part of the Fermi arc attached to the bulk, as illustrated in Fig. 1(a). Hence, considerable bulk-Fermi-arc transition should widely occur in WSMs [52–54]. Besides, bulk-surface-state transition can also happen in topological insulators with certain surface doping [55–57].

We first establish a local second-order response formula of the shift conductivities, and then use it to study the sur-

<sup>\*</sup>These authors contributed equally to this work.

<sup>†</sup>zhiming\_yu@bit.edu.cn

<sup>‡</sup>ygyao@bit.edu.cn

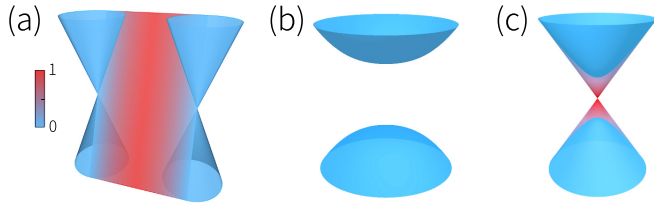


FIG. 1. Three typical band structures. (a) Weyl semimetal with surface Fermi arc. (b) Trivial insulator and (c) topological insulator with topological surface state. The blue surfaces denote bulk bands. The surface states in (a) and (c) are attached to the bulk bands. The color map in surface states indicates the weight of projection onto one surface. Considerable transition between bulk and surface states widely appears in (a), while cannot happen for (b), and happen in (c) for certain doping.

face shift current of a centrosymmetric WSM with two Weyl points. In this WSM model, both the bulk shift current and the surface shift current, solely from the surface Fermi arc, are zero. Surprisingly, we find that significant surface shift current effect still occurs, and only occurs on the boundaries with Fermi arc, indicating that this considerable large shift current is induced by the bulk-Fermi-arc transition. Particularly, the absolute value of the effective surface shift conductivities induced by the bulk-Fermi-arc transition can exceed  $100 \mu\text{A}/\text{V}^2$  in a wide terahertz range for different Fermi energy. Such large shift current is comparable with that in the single-layer monochalcogenides [28] and the bulk shift current in the previously studied topological semimetals [38]. More importantly, due to the low symmetry on the boundary, the surface shift current effect predicted here generally would appear in all kinds of the WSMs, including a large class of WSMs that do not have net shift current in bulk. Thus, by unveiling a hidden photogalvanic effect in WSMs, our work proposes a promising route to design terahertz photodetectors, which not only takes the advantage of the gapless feature of the Fermi arc [58], but also effectively circumvents the restrictions imposed by the bulk symmetries of the WSMs.

## II. LOCAL PHOTOCURRENT RESPONSE

We first establish a general formula to describe the local photocurrent response in the independent particle approximation. The space dependent current operator generally can be written as [59]

$$J^a(\mathbf{r}) = -\frac{e}{2V} \sum_{\mu\nu, r'} v_{\mu r, \nu r'}^a d_{\mu r}^\dagger d_{\nu r'} + \text{H.c.}, \quad (2)$$

which counts all of the currents flowing from  $\mathbf{r}'$  to  $\mathbf{r}$ . Here,  $V$  is the volume of system,  $e$  denotes the charge carried by an electron,  $d_{\mu r}^\dagger$  ( $d_{\mu r}$ ) creates (annihilates) a localized Wannier state  $w_{\mu r}$  at  $\mathbf{r}$  with basis orbit  $\mu$ , and  $v_{\mu r, \nu r'}^a = \frac{1}{2m} \langle w_{\mu r} | -i\partial_a | w_{\nu r'} \rangle$  with  $m$  the electronic mass. The eigenstates are constructed from the Wannier states by  $c_n^\dagger = \sum_{\mu r} U_{\mu r, n} d_{\mu r}^\dagger$  with  $n$  a combined index denoting energy band and momentum (if the system has translation symmetry), it then follows

$$J^a(\mathbf{r}) = -\frac{e}{V} \sum_{mn} v_{mn, r}^a c_m^\dagger c_n, \quad (3)$$

where  $v_{mn, r}^a$  is the local velocity operator matrix, defined as

$$v_{mn, r}^a \equiv \frac{1}{2} \sum_{\mu\nu, r'} U_{m, \mu r}^\dagger v_{\mu r, \nu r'}^a U_{\nu r', n} + \text{H.c.} \quad (4)$$

Here, we focus on the surface shift conductivities induced by a linearly polarized light. Consider a slab model with  $y$ -direction being confined ( $y \in [-\frac{L}{2}, \frac{L}{2}]$ ) and assuming the model is illuminated by a monochromatic light of frequency  $\omega$ . The applied light (electric) field is introduced into the Hamiltonian by velocity-gauge approach,  $H' = -\int d\mathbf{r} \mathbf{J}(\mathbf{r}) \cdot \mathbf{A}(\mathbf{r}, t)$ . According to the standard perturbation procedure, the local shift conductivity can be established as [60]

$$\sigma_{bc}^a(\omega; y) = -\frac{\pi e^3}{2L\omega^2} \text{Im} \int \frac{dk_x dk_z}{(2\pi)^2} \sum_{y', y''} \sum_{l \neq m, n; \pm\omega} \frac{f_{nl}}{\varepsilon_{lm}} \times v_{lm, y}^a (v_{mn, y'}^b v_{nl, y''}^c + v_{mn, y''}^c v_{nl, y'}^b) \delta(\varepsilon_{ln} - \hbar\omega), \quad (5)$$

where  $f_{nl} = f_n - f_l$  and  $\varepsilon_{lm} = \varepsilon_l - \varepsilon_m$  are the occupation and the energy differences between the states involved in the optical transition,  $f_n$  is the Fermi-Dirac distribution. Clearly, the shift current effect is a interband effect, as Eq. (5) has the form of Fermi golden rule.

There are several remarks for the bulk-Fermi-arc transition based on Eq. (5). (i) For the WSMs with one Fermi arc on one certain boundary, the shift current effect involving the Fermi arc must be induced by bulk-Fermi-arc transition. (ii) Since the Fermi arc can have sizable overlap between the bulk states,  $v_{lm, y=\pm L/2}^a$  and then  $\sigma_{bc}^a(\omega; \pm L/2)$ , generally are finite for bulk-Fermi-arc transition. (iii) Particularly, the gapless feature of the Fermi arc guarantees that the bulk-Fermi-arc transition induced shift conductivities would be significantly enhanced in (and only in) terahertz range. Moreover, the enhanced surface shift conductivities only respect the magnetic point group symmetries of the corresponding boundary, rather than the symmetries of bulk.

For top surface, the effective three-dimensional (3D) shift conductivity may be defined as

$$\Sigma_{bc}^a(\omega) = \frac{1}{l} \int_{L/2-l}^{L/2} dy \sigma_{bc}^a(\omega; y), \quad (6)$$

where  $l \ll L$ . The conductivity for bottom surface can be similarly defined. While  $\Sigma_{bc}^a(\omega)$  generally depends on both  $L$  and  $l$  [61], its qualitative behaviors would be robust against the choice of  $L$  and  $l$ .

## III. WEYL MODEL

We take a simple WSM model to demonstrate that the bulk-Fermi-arc transition can generate large optical responses. The WSM model contains only two Weyl points (without energy tilt) at the Fermi level. The essential physics learned here applies to general WSMs and other topological semimetals with robust surface Fermi arc. We also assume the system has  $\mathcal{P}$  symmetry to exclude the bulk photocurrent. This indicates the WSM model has to break time-reversal symmetry ( $\mathcal{T}$ ). Since there exists (at most) only one surface Fermi arc on each boundary of system, the surface shift conductivity solely from the Fermi arc would be zero.

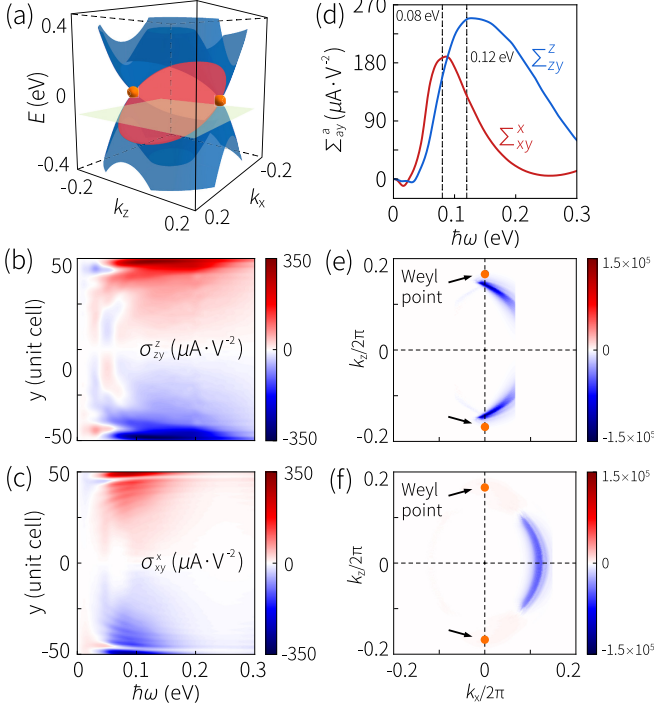


FIG. 2. (a) Band structure of the model (7) at  $k_y = 0$  plane (blue surfaces), together with the surface Fermi arc at (010) surface (red surface). Green plane denotes Fermi level. (b), (c) show the local shift conductivity  $\sigma_{zy}^z(\omega; y)$  and  $\sigma_{xy}^x(\omega; y)$  for the (010) slab, where significant surface enhancement can be observed. We set  $E_F = -0.1$  eV in (b),  $E_F = -0.2$  eV in (c). (d) shows the two surface shift conductivities which are obtained from (b) and (c) with  $l = 4L_s$ . (e), (f) The distribution of  $\Sigma_{zy}^z(\omega)$  and  $\Sigma_{xy}^x(\omega)$  in the (010) surface BZ. We set  $E_F = -0.1$  eV and  $\hbar\omega = 0.12$  eV in (e), and  $E_F = -0.2$  eV and  $\hbar\omega = 0.08$  eV in (f). The sharp cutoff in (e), (f) and Fig. 5(b) are due to the abrupt change in Fermi-Dirac distribution at zero temperature.

The WSM model is defined on a cubic lattice

$$\mathcal{H}_W(\mathbf{k}) = [\Delta + t_1(\cos k_x + \cos k_y) + t_2 \cos k_z] \sigma_z + t_3(\sin k_x \sigma_x + \sin k_y \sigma_y), \quad (7)$$

where  $\sigma_i$ 's are the Pauli matrices,  $t_1 = t_2 = 1.0$  eV,  $t_3 = 0.25$  eV, and  $\Delta = \Delta_0 - 2t_1 - t_2$  with  $\Delta_0 = 0.5$  eV. The model (7) has only two Weyl points with Chern number  $C = \pm 1$  on the  $k_z$  axis at  $k_z^\pm = \pm \arccos(2\Delta_0/t_1)$ . In the bulk, the symmetries of the lattice model are generated by  $\mathcal{P}$  symmetry, a mirror  $\mathcal{M}_z$ , a fourfold rotation  $\mathcal{C}_{4z}$  and a combined operator  $\mathcal{C}_{2y}\mathcal{T}$ , which, respectively, can be represented as  $\mathcal{P} = \sigma_z$ ,  $\mathcal{M}_z = i\sigma_0$ ,  $\mathcal{C}_{4z} = \frac{\sigma_0 + i\sigma_z}{\sqrt{2}}$ , and  $\mathcal{C}_{2y}\mathcal{T} = \mathcal{K}$  with  $\sigma_0$  the two-dimensional identity matrix.

The calculated band structure from Eq. (7) is plotted in Fig. 2(a) together with the surface Fermi arc on the (010) surface. Two Weyl cones residing at  $k_z^\pm \hat{z}$  points are observed. They are connected to each other at higher (lower) energy, forming a saddle surface around the  $k_x$  axis. The surface Fermi arc is attached to the two Weyl cones at low energy, and merges into the bulk saddle surface at higher (lower) energy. Hence, there exists a critical line in WSMs [58] which separates the surface Fermi arc states from the bulk states [see Fig. 2(a)]. Only around the critical line, the bulk-Fermi-arc

transitions would be significant. Moreover, since the critical line has an energy variation [see Fig. 2(a)], the bulk-Fermi-arc transitions will occur around different regions for different Fermi energy.

#### IV. SURFACE SHIFT CURRENT

We first study the shift current on the (010) surface of the lattice model (7). Following calculations are performed at zero temperature. The nonzero components of the surface shift conductivity tensors are determined by the magnetic point group of the (010) surface, which are generated by  $\mathcal{M}_z$  and  $\mathcal{C}_{2y}\mathcal{T}$ . Then the shift conductivity tensors, that are odd under the mirror  $\mathcal{M}_z$ , namely,  $\sigma_{xz}^x$ ,  $\sigma_{yz}^x$ ,  $\sigma_{xx}^z$ ,  $\sigma_{yy}^z$ ,  $\sigma_{zz}^z$ ,  $\sigma_{xy}^z$ ,  $\sigma_{xz}^z$ , and  $\sigma_{yz}^z$  vanish. Similarly,  $\sigma_{xx}^x$ ,  $\sigma_{yy}^x$ ,  $\sigma_{zz}^x$ , and  $\sigma_{xz}^x$  are excluded by  $\mathcal{C}_{2y}\mathcal{T}$ . Thus, there are only four symmetry allowed tensors, and two of them are independent, which are  $\sigma_{xy}^x = \sigma_{yx}^x$  and  $\sigma_{zy}^z = \sigma_{yz}^z$ .

Using formula (5), we calculate the local shift conductivities  $\sigma_{zy}^z(\omega; y)$  and  $\sigma_{xy}^x(\omega; y)$  for a (010) slab with a thickness of  $L = 101 L_s$ . Here,  $L_s$  is the thickness of a unit cell. We find that  $\sigma_{zy}^z(\omega; y)$  [ $\sigma_{xy}^x(\omega; y)$ ] is large when the Fermi level is close to (away from) the Weyl point [60]. Figure 2(b) shows the results of  $\sigma_{zy}^z(\omega; y)$  for  $E_F = -0.1$  eV, and Fig. 2(c) shows the results of  $\sigma_{xy}^x(\omega; y)$  for  $E_F = -0.2$  eV. Both  $\sigma_{xy}^x(\omega; y)$  and  $\sigma_{zy}^z(\omega; y)$  are finite for a generic layer of the slab. This is because the slab studied here is not thick enough. Surprisingly, the two conductivities feature strong surface-enhancing behavior in low frequency regions, leading to significant photogalvanic effect on the (010) surface.

For clarity, we calculate the effective 3D shift conductivities on the (010) surface:  $\Sigma_{xy}^x(\omega)$  and  $\Sigma_{zy}^z(\omega)$ , with  $l = 4L_s$ , and find that these two conductivities can be larger than  $100 \mu\text{A}/\text{V}^2$  in a wide frequency range, as shown in Fig. 2(d). Such large surface shift conductivities, to our best knowledge, has never been reported before. Moreover, the peak of both  $\Sigma_{xy}^x(\omega)$  and  $\Sigma_{zy}^z(\omega)$  appear around terahertz range ( $\hbar\omega \sim 100$  meV). Thus, the surface photogalvanic effect predicted here can be used to design efficient terahertz photodetectors.

As discussed above, such large surface optical responses in terahertz range should be caused by the bulk-Fermi-arc transition. To further demonstrate it, we calculate the distribution of the effective conductivities  $\Sigma_{zy}^z(\omega)$  and  $\Sigma_{xy}^x(\omega)$  in the 2D Brillouin zone (BZ) of the (010) slab. The results are shown in Figs. 2(e) and 2(f). Interestingly, the distribution for both conductivities concentrates around the critical line, directly showing that the bulk-Fermi-arc transitions can induce significant enhancement of the surface shift conductivities. Moreover, as a nature feature, the bulk-Fermi-arc transition induced enhancement only appears in terahertz range [60]. From Figs. 2(e) and 2(f), one finds that the large contribution for  $\Sigma_{zy}^z(\omega)$  comes from the transition between the two Weyl points and the Fermi arc, while for  $\Sigma_{xy}^x(\omega)$  it is from the transition between the saddle surface and the arc. Both transitions are bulk-Fermi-arc transitions but occur at two different parts of the critical line. This difference will lead to completely different behaviors of  $\Sigma_{zy}^z(\omega)$  and  $\Sigma_{xy}^x(\omega)$ .

When the Fermi level exactly locates at Weyl points  $E_F = 0$ , the model (7) has an emergent particle-hole symmetry  $\mathcal{C} = \sigma_x \mathcal{K}$  with  $\mathcal{C}\mathcal{H}_W(\mathbf{k})\mathcal{C}^{-1} = -\mathcal{H}_W(-\mathbf{k})$ ; in such a case,

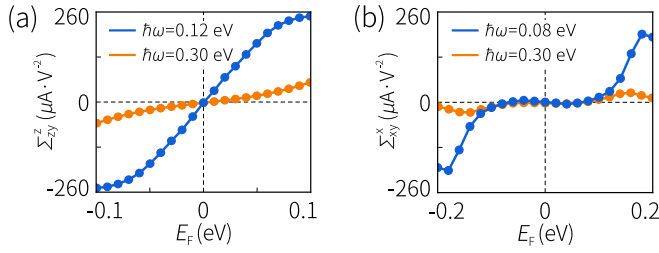


FIG. 3. The (010) surface shift conductivities (a)  $\Sigma_{zy}^z$  and (b)  $\Sigma_{xy}^x$  of the Weyl model (7) versus the Fermi level. When  $\hbar\omega$  becomes large, the effect of the bulk-Fermi-arc transition would be strongly suppressed.

all the shift conductivities would vanish, as the particle-hole symmetry reverses the direction of the photocurrent [20].

Deviating from the neutral filling point, the absolute value of  $\Sigma_{zy}^z(\omega)$  will increase rapidly [see Fig. 3(a)], as the transition between the two Weyl points and the attached Fermi arc will occur. In contrast, the transition between the saddle surface and the Fermi arc near  $k_x$  axis are absent when  $E_F$  is small, and appears only when the Fermi level approaches the bulk saddle surface [see Fig. 2(a)]. Hence,  $\Sigma_{xy}^x(\omega)$  will still be almost vanishing for  $|E_F| < 0.1$  eV, and becomes large when  $|E_F| \simeq 0.2$  eV [see Fig. 3(b)]. We also calculate the  $\Sigma_{zy}^z(\omega)$  and  $\Sigma_{xy}^x(\omega)$  for higher frequency of light  $\hbar\omega = 0.3$  eV, and find both conductivities are negligible (see Fig. 3), consistent with the feature of the Bulk-Fermi-arc transitions.

For comparison, we then study the local shift conductivities on the (001) surface of the WSM model (7) under the same parameters. For (001) surface, only one shift current conductivity  $\sigma_{xz}^x(\omega; z)$  is independent [60]. Unlike the (010) surface, the (001) surface does not have a Fermi arc because the two Weyl points are projected to the same point in the 2D BZ of the (001) surface [see Fig. 4(a)]. We find that for different  $\hbar\omega$  and  $E_F$ , the  $\sigma_{xz}^x(\omega; z)$  does not feature significant surface-enhancing behavior, and the obtained effective shift conductivity on (001) surface [ $\Sigma_{xz}^x(\omega; z)$ ] is much smaller than that on (010) surface, as shown in Figs. 4(b) and 4(c). These results unambiguously demonstrates that the significant surface photogalvanic effect in WSMs can be induced by the bulk-Fermi-arc transition.

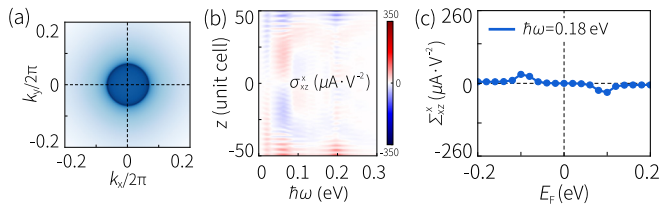


FIG. 4. (a) Surface spectra on (001) surface of the lattice model (7). (b) The local shift conductivity  $\sigma_{xz}^x(\omega; z)$  for the (001) slab. In (a) and (b), we set  $E_F = -0.1$  eV. (c) The (001) surface shift conductivity versus the Fermi level.

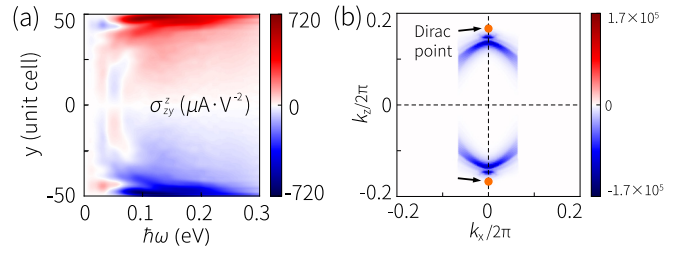


FIG. 5. (a) The local shift conductivity  $\sigma_{zy}^z(\omega; y)$  for the (010) slab of the Dirac model (8). (b) shows the distribution of  $\Sigma_{zy}^z(\omega)$  in the (010) surface BZ. We set  $c_1 = c_2 = 0.1$  eV,  $E_F = -0.1$  eV in (a) and (b), and set  $\hbar\omega = 0.12$  eV in (b).

## V. DISCUSSIONS

Here, we demonstrate that the bulk-Fermi-arc transition can induce large surface photovoltaic effect in WSMs. Actually, this effect may exist in all the topological semimetals with surface Fermi arc. As an example, we consider a Dirac semimetal. Generally, the surface state of a Dirac semimetal is topologically trivial [62], but under suitable boundary conditions, it can be gapless and contains two Fermi arc surface states [63,64]. The Dirac Hamiltonian may be written as

$$\mathcal{H}_D(\mathbf{k}) = \begin{bmatrix} \mathcal{H}_W(\mathbf{k}) & h_1 + h_2 \\ h_1^\dagger + h_2^\dagger & \mathcal{H}_W^*(-\mathbf{k}) \end{bmatrix}, \quad (8)$$

where  $h_1 = -2c_1(\cos k_x - \cos k_y) \sin k_z \sigma_x$ ,  $h_2 = -ic_2 \sin k_x \sin k_y \sin k_z \sigma_x$ , and  $\mathcal{H}_W(\mathbf{k})$  is defined in Eq. (7). This model has  $\mathcal{P}$  and  $\mathcal{T}$  symmetry, and gives a pair of Dirac points at  $k_z$  axis. There exist two Fermi arcs on the (010) surface, which, respectively, occupy different parts of the (010) surface BZ [60]. Thus, for model (8), the shift current, solely from both the bulk and the surface Fermi arcs, vanish. The symmetry allowed independent tensors on the (010) surface are  $\sigma_{xy}^x = \sigma_{yx}^x$  and  $\sigma_{zy}^z = \sigma_{yz}^z$  [60].

The calculated results of  $\sigma_{zy}^z(\omega; y)$  for the (010) slab of the Dirac model (8) are given in Fig. 5. Similar to the cases in WSM (7),  $\sigma_{zy}^z(\omega; y)$  here also exhibits strong surface enhancement and the distribution of  $\Sigma_{zy}^z(\omega)$  mainly concentrates around the critical line, which, here separate the two Fermi arc states and the bulk states. The results for  $\sigma_{zy}^z(\omega; y)$  are similar [60]. These calculations show the bulk-Fermi-arc transition indeed can generate significant surface photovoltaic effects in Dirac semimetals.

The experimental detection of the surface shift current effect has been well developed [39,65], and many materials are experimentally confirmed as topological (Weyl) semimetals [66–73]. Particularly, Rees *et al.* [50] experimentally measured the surface photogalvanic effect in RhSi with the incident photon energy ranging from 0.45 eV to 1.1 eV, and the results are well consistent with the theoretical predictions [49]. Hence, in a similar setup but with lower photon energy, the novel effect predicted here should be probed.

## ACKNOWLEDGMENTS

The authors thank S. A. Yang, Rui-Chun Xiao, and J. Xun for helpful discussions. This work is supported

by the National Key R&D Program of China (Grant No. 2020YFA0308800), the NSF of China (Grants No. 12004035, No. 11734003, and No. 12061131002), the Strategic Priority

Research Program of Chinese Academy of Sciences (Grant No. XDB30000000), and Beijing Institute of Technology Research Fund Program for Young Scholars.

- 
- [1] R. W. Boyd, *Nonlinear Optics* (Academic Press, San Diego, 1992).
- [2] S. M. Young and A. M. Rappe, First Principles Calculation of the Shift Current Photovoltaic Effect in Ferroelectrics, *Phys. Rev. Lett.* **109**, 116601 (2012).
- [3] S. M. Young, F. Zheng, and A. M. Rappe, First-Principles Calculation of the Bulk Photovoltaic Effect in Bismuth Ferrite, *Phys. Rev. Lett.* **109**, 236601 (2012).
- [4] C. Somma, K. Reimann, C. Flytzanis, T. Elsaesser, and M. Woerner, High-Field Terahertz Bulk Photovoltaic Effect in Lithium Niobate, *Phys. Rev. Lett.* **112**, 146602 (2014).
- [5] M. Nakamura, S. Horiuchi, F. Kagawa, N. Ogawa, T. Kurumaji, Y. Tokura, and M. Kawasaki, Shift current photovoltaic effect in a ferroelectric charge-transfer complex, *Nat. Commun.* **8**, 281 (2017).
- [6] C. Wang, X. Liu, L. Kang, B.-L. Gu, Y. Xu, and W. Duan, First-principles calculation of nonlinear optical responses by wannier interpolation, *Phys. Rev. B* **96**, 115147 (2017).
- [7] A. Ghalgaoui, K. Reimann, M. Woerner, T. Elsaesser, C. Flytzanis, and K. Biermann, Resonant Second-Order Nonlinear Terahertz Response of Gallium Arsenide, *Phys. Rev. Lett.* **121**, 266602 (2018).
- [8] Y. Zhang, T. Holder, H. Ishizuka, F. de Juan, N. Nagaosa, C. Felser, and B. Yan, Switchable magnetic bulk photovoltaic effect in the two-dimensional magnet CrI<sub>3</sub>, *Nat. Commun.* **10**, 3783 (2019).
- [9] A. M. Burger, R. Agarwal, A. Aprelev, E. Schrubba, A. Gutierrez-Perez, V. M. Fridkin, and J. E. Spanier, Direct observation of shift and ballistic photovoltaic currents, *Sci. Adv.* **5**, eaau5588 (2019).
- [10] S. R. Panday, S. Barraza-Lopez, T. Rangel, and B. M. Fregoso, Injection current in ferroelectric group-iv monochalcogenide monolayers, *Phys. Rev. B* **100**, 195305 (2019).
- [11] H. Wang and X. Qian, Ferroicity-driven nonlinear photocurrent switching in time-reversal invariant ferroic materials, *Sci. Adv.* **5**, eaav9743 (2019).
- [12] R.-C. Xiao, D.-F. Shao, Y.-H. Li, and H. Jiang, Spin photogalvanic effect in two-dimensional collinear antiferromagnets, *npj Quantum Mater.* **6**, 35 (2021).
- [13] J. E. Sipe and A. I. Shkrebti, Second-order optical response in semiconductors, *Phys. Rev. B* **61**, 5337 (2000).
- [14] T. Morimoto, S. Zhong, J. Orenstein, and J. E. Moore, Semiclassical theory of nonlinear magneto-optical responses with applications to topological dirac/weyl semimetals, *Phys. Rev. B* **94**, 245121 (2016).
- [15] T. Morimoto and N. Nagaosa, Topological nature of nonlinear optical effects in solids, *Sci. Adv.* **2**, e1501524 (2016).
- [16] N. Nagaosa and T. Morimoto, Concept of quantum geometry in optoelectronic processes in solids: Application to solar cells, *Adv. Mater.* **29**, 1603345 (2017).
- [17] B. M. Fregoso, T. Morimoto, and J. E. Moore, Quantitative relationship between polarization differences and the zone-averaged shift photocurrent, *Phys. Rev. B* **96**, 075421 (2017).
- [18] B. M. Fregoso, R. A. Muniz, and J. E. Sipe, Jerk Current: A Novel Bulk Photovoltaic Effect, *Phys. Rev. Lett.* **121**, 176604 (2018).
- [19] D. E. Parker, T. Morimoto, J. Orenstein, and J. E. Moore, Diagrammatic approach to nonlinear optical response with application to weyl semimetals, *Phys. Rev. B* **99**, 045121 (2019).
- [20] J. Ahn, G.-Y. Guo, and N. Nagaosa, Low-Frequency Divergence and Quantum Geometry of the Bulk Photovoltaic Effect in Topological Semimetals, *Phys. Rev. X* **10**, 041041 (2020).
- [21] T. Holder, D. Kaplan, and B. Yan, Consequences of time-reversal-symmetry breaking in the light-matter interaction: Berry curvature, quantum metric, and diabatic motion, *Phys. Rev. Res.* **2**, 033100 (2020).
- [22] P. Bhalla, A. H. MacDonald, and D. Culcer, Resonant Photovoltaic Effect in Doped Magnetic Semiconductors, *Phys. Rev. Lett.* **124**, 087402 (2020).
- [23] B. I. Sturman, Ballistic and shift currents in the bulk photovoltaic effect theory, *Phys. Usp.* **63**, 407 (2020).
- [24] J. Liu, F. Xia, D. Xiao, F. J. García de Abajo, and D. Sun, Semimetals for high-performance photodetection, *Nat. Mater.* **19**, 830 (2020).
- [25] N. Nagaosa, T. Morimoto, and Y. Tokura, Transport, magnetic and optical properties of weyl materials, *Nat. Rev. Mater.* **5**, 621 (2020).
- [26] L. Z. Tan, F. Zheng, S. M. Young, F. Wang, S. Liu, and A. M. Rappe, Shift current bulk photovoltaic effect in polar materials—hybrid and oxide perovskites and beyond, *npj Comput. Mater.* **2**, 16026 (2016).
- [27] A. M. Cook, B. M. Fregoso, F. de Juan, S. Coh, and J. E. Moore, Design principles for shift current photovoltaics, *Nat. Commun.* **8**, 14176 (2017).
- [28] T. Rangel, B. M. Fregoso, B. S. Mendoza, T. Morimoto, J. E. Moore, and J. B. Neaton, Large Bulk Photovoltaic Effect and Spontaneous Polarization of Single-Layer Monochalcogenides, *Phys. Rev. Lett.* **119**, 067402 (2017).
- [29] H. Ishizuka, T. Hayata, M. Ueda, and N. Nagaosa, Emergent Electromagnetic Induction and Adiabatic Charge Pumping in Noncentrosymmetric Weyl Semimetals, *Phys. Rev. Lett.* **117**, 216601 (2016).
- [30] K. Taguchi, T. Imaeda, M. Sato, and Y. Tanaka, Photovoltaic chiral magnetic effect in weyl semimetals, *Phys. Rev. B* **93**, 201202(R) (2016).
- [31] F. de Juan, A. G. Grushin, T. Morimoto, and J. E. Moore, Quantized circular photogalvanic effect in weyl semimetals, *Nat. Commun.* **8**, 15995 (2017).
- [32] C.-K. Chan, N. H. Lindner, G. Refael, and P. A. Lee, Photocurrents in weyl semimetals, *Phys. Rev. B* **95**, 041104(R) (2017).
- [33] E. J. König, H.-Y. Xie, D. A. Pesin, and A. Levchenko, Photogalvanic effect in weyl semimetals, *Phys. Rev. B* **96**, 075123 (2017).
- [34] Q. Ma, S.-Y. Xu, C.-K. Chan, C.-L. Zhang, G. Chang, Y. Lin, W. Xie, T. Palacios, H. Lin, S. Jia, P. A. Lee, P.

- Jarillo-Herrero, and N. Gedik, Direct optical detection of weyl fermion chirality in a topological semimetal, *Nat. Phys.* **13**, 842 (2017).
- [35] F. Flicker, F. de Juan, B. Bradlyn, T. Morimoto, M. G. Vergniory, and A. G. Grushin, Chiral optical response of multi-fold fermions, *Phys. Rev. B* **98**, 155145 (2018).
- [36] L. E. Golub and E. L. Ivchenko, Circular and magnetoinduced photocurrents in weyl semimetals, *Phys. Rev. B* **98**, 075305 (2018).
- [37] T. Morimoto, M. Nakamura, M. Kawasaki, and N. Nagaosa, Current-Voltage Characteristic and Shot Noise of Shift Current Photovoltaics, *Phys. Rev. Lett.* **121**, 267401 (2018).
- [38] Y. Zhang, H. Ishizuka, J. van den Brink, C. Felser, B. Yan, and N. Nagaosa, Photogalvanic effect in weyl semimetals from first principles, *Phys. Rev. B* **97**, 241118(R) (2018).
- [39] Q. Wang, J. Zheng, Y. He, J. Cao, X. Liu, M. Wang, J. Ma, J. Lai, H. Lu, S. Jia, D. Yan, Y. Shi, J. Duan, J. Han, W. Xiao, J.-H. Chen, K. Sun, Y. Yao, and D. Sun, Robust edge photocurrent response on layered type II Weyl semimetal WTe<sub>2</sub>, *Nat. Commun.* **10**, 5736 (2019).
- [40] G. B. Osterhoudt, L. K. Diebel, M. J. Gray, X. Yang, J. Stanco, X. Huang, B. Shen, N. Ni, P. J. Moll, Y. Ran *et al.*, Colossal mid-infrared bulk photovoltaic effect in a type-I Weyl semimetal, *Nat. Mater.* **18**, 471 (2019).
- [41] J. Ma, Q. Gu, Y. Liu, J. Lai, P. Yu, X. Zhuo, Z. Liu, J.-H. Chen, J. Feng, and D. Sun, Nonlinear photoresponse of type-II weyl semimetals, *Nat. Mater.* **18**, 476 (2019).
- [42] D. Rees, K. Manna, B. Lu, T. Morimoto, H. Borrmann, C. Felser, J. E. Moore, D. H. Torchinsky, and J. Orenstein, Helicity-dependent photocurrents in the chiral weyl semimetal rhsi, *Sci. Adv.* **6**, eaba0509 (2020).
- [43] K. Halterman, M. Alidoust, and A. Zyuzin, Epsilon-near-zero response and tunable perfect absorption in weyl semimetals, *Phys. Rev. B* **98**, 085109 (2018).
- [44] N. P. Armitage, E. J. Mele, and A. Vishwanath, Weyl and dirac semimetals in three-dimensional solids, *Rev. Mod. Phys.* **90**, 015001 (2018).
- [45] G. Chang, B. J. Wieder, F. Schindler, D. S. Sanchez, I. Belopolski, S.-M. Huang, B. Singh, D. Wu, T.-R. Chang, T. Neupert, S.-Y. Xu, H. Lin, and M. Z. Hasan, Topological quantum properties of chiral crystals, *Nat. Mater.* **17**, 978 (2018).
- [46] Z.-M. Yu, Z. Zhang, G.-B. Liu, W. Wu, X.-P. Li, R.-W. Zhang, S. A. Yang, and Y. Yao, Encyclopedia of emergent particles in three-dimensional crystals, *Sci. Bull.* **67**, 375 (2022).
- [47] X. Wan, A. M. Turner, A. Vishwanath, and S. Y. Savrasov, Topological semimetal and fermi-arc surface states in the electronic structure of pyrochlore iridates, *Phys. Rev. B* **83**, 205101 (2011).
- [48] C. Cui, X.-P. Li, D.-S. Ma, Z.-M. Yu, and Y. Yao, Charge-four weyl point: Minimum lattice model and chirality-dependent properties, *Phys. Rev. B* **104**, 075115 (2021).
- [49] G. Chang, J.-X. Yin, T. Neupert, D. S. Sanchez, I. Belopolski, S. S. Zhang, T. A. Cochran, Z. c. v. b. a. Chéng, M.-C. Hsu, S.-M. Huang, B. Lian, S.-Y. Xu, H. Lin, and M. Z. Hasan, Unconventional Photocurrents from Surface Fermi Arcs in Topological Chiral Semimetals, *Phys. Rev. Lett.* **124**, 166404 (2020).
- [50] D. Rees, B. Lu, Y. Sun, K. Manna, R. Özgür, S. Subedi, H. Borrmann, C. Felser, J. Orenstein, and D. H. Torchinsky, Direct Measurement of Helicoid Surface States in RhSi Using Nonlinear Optics, *Phys. Rev. Lett.* **127**, 157405 (2021).
- [51] S. Chi, F. Liang, H. Chen, W. Tian, H. Zhang, H. Yu, G. Wang, Z. Lin, J. Hu, and H. Zhang, Surface nonlinear optics on centrosymmetric dirac nodal-line semimetal zrsis, *Adv. Mater.* **32**, 1904498 (2020).
- [52] A. C. Potter, I. Kimchi, and A. Vishwanath, Quantum oscillations from surface fermi arcs in weyl and dirac semimetals, *Nat. Commun.* **5**, 5161 (2014).
- [53] C. M. Wang, H.-P. Sun, H.-Z. Lu, and X. C. Xie, 3D Quantum Hall Effect of Fermi Arcs in Topological Semimetals, *Phys. Rev. Lett.* **119**, 136806 (2017).
- [54] E. V. Gorbar, V. A. Miransky, I. A. Shovkovy, and P. O. Sukhachov, Origin of dissipative fermi arc transport in weyl semimetals, *Phys. Rev. B* **93**, 235127 (2016).
- [55] H. Plank and S. D. Ganichev, A review on terahertz photogalvanic spectroscopy of Bi<sub>2</sub>Te<sub>3</sub>- and Sb<sub>2</sub>Te<sub>3</sub>-based three dimensional topological insulators, *Solid-State Electron.* **147**, 44 (2018).
- [56] H. Plank, J. Pernul, S. Gebert, S. N. Danilov, J. König-Otto, S. Winnerl, M. Lanius, J. Kampmeier, G. Mussler, I. Aguilera, D. Grützmacher, and S. D. Ganichev, Infrared/terahertz spectra of the photogalvanic effect in (bi, sb)te based three-dimensional topological insulators, *Phys. Rev. Mater.* **2**, 024202 (2018).
- [57] S. N. Danilov, L. E. Golub, T. Mayer, A. Beer, S. Binder, E. Mönch, J. Minár, M. Kronseder, C. H. Back, D. Bougeard, and S. D. Ganichev, Superlinear Photogalvanic Effects in (Bi<sub>0.3</sub>Sb<sub>0.7</sub>)<sub>2</sub>(Te<sub>0.1</sub>Se<sub>0.9</sub>)<sub>3</sub>: Probing Three-Dimensional Topological Insulator Surface States at Room Temperature, *Phys. Rev. Appl.* **16**, 064030 (2021).
- [58] D. Wawrzik, J.-S. You, J. I. Facio, J. van den Brink, and I. Sodemann, Infinite Berry Curvature of Weyl Fermi Arcs, *Phys. Rev. Lett.* **127**, 056601 (2021).
- [59] G. D. Mahan, *Many-Particle Physics*, 3rd. ed. (Springer Science & Business Media, New York, 2000).
- [60] See Supplemental Material at <http://link.aps.org/supplemental/10.1103/PhysRevB.106.125416> for the details about the derivation of Eq. (5), the detailed analyses of the shift conductivities on (010) surface, the shift conductivities on (001) surface, and the symmetry analysis of the Dirac model.
- [61] O. Pozo, C. Repellin, and A. G. Grushin, Quantization in Chiral Higher Order Topological Insulators: Circular Dichroism and Local Chern Marker, *Phys. Rev. Lett.* **123**, 247401 (2019).
- [62] M. Kargarian, M. Randeria, and Y.-M. Lu, Are the surface fermi arcs in dirac semimetals topologically protected?, *Proc. Natl. Acad. Sci.* **113**, 8648 (2016).
- [63] Z. Wang, Y. Sun, X.-Q. Chen, C. Franchini, G. Xu, H. Weng, X. Dai, and Z. Fang, Dirac semimetal and topological phase transitions in A<sub>3</sub>bi (*a* = Na, k, rb), *Phys. Rev. B* **85**, 195320 (2012).
- [64] Z. Wang, H. Weng, Q. Wu, X. Dai, and Z. Fang, Three-dimensional dirac semimetal and quantum transport in Cd<sub>3</sub>As<sub>2</sub>, *Phys. Rev. B* **88**, 125427 (2013).
- [65] Y. Q. Huang, Y. X. Song, S. M. Wang, I. A. Buyanova, and W. M. Chen, Spin injection and helicity control of surface spin photocurrent in a three dimensional topological insulator, *Nat. Commun.* **8**, 15401 (2017).

- [66] B. Q. Lv, T. Qian, and H. Ding, Experimental perspective on three-dimensional topological semimetals, *Rev. Mod. Phys.* **93**, 025002 (2021).
- [67] G. Chang, S.-Y. Xu, B. J. Wieder, D. S. Sanchez, S.-M. Huang, I. Belopolski, T.-R. Chang, S. Zhang, A. Bansil, H. Lin, and M. Z. Hasan, Unconventional Chiral Fermions and Large Topological Fermi Arcs in RhSi, *Phys. Rev. Lett.* **119**, 206401 (2017).
- [68] M. Neupane, S.-Y. Xu, R. Sankar, N. Alidoust, G. Bian, C. Liu, I. Belopolski, T.-R. Chang, H.-T. Jeng, H. Lin, A. Bansil, F. Chou, and M. Z. Hasan, Observation of a three-dimensional topological dirac semimetal phase in high-mobility Cd<sub>3</sub>As<sub>2</sub>, *Nat. Commun.* **5**, 3786 (2014).
- [69] S.-Y. Xu, C. Liu, S. K. Kushwaha, R. Sankar, J. W. Krizan, I. Belopolski, M. Neupane, G. Bian, N. Alidoust, T.-R. Chang, H.-T. Jeng, C.-Y. Huang, W.-F. Tsai, H. Lin, P. P. Shibayev, F.-C. Chou, R. J. Cava, and M. Z. Hasan, Observation of fermi arc surface states in a topological metal, *Science* **347**, 294 (2015).
- [70] B. Q. Lv, S. Muff, T. Qian, Z. D. Song, S. M. Nie, N. Xu, P. Richard, C. E. Matt, N. C. Plumb, L. X. Zhao, G. F. Chen, Z. Fang, X. Dai, J. H. Dil, J. Mesot, M. Shi, H. M. Weng, and H. Ding, Observation of Fermi-Arc Spin Texture in TaAs, *Phys. Rev. Lett.* **115**, 217601 (2015).
- [71] K. Deng, G. Wan, P. Deng, K. Zhang, S. Ding, E. Wang, M. Yan, H. Huang, H. Zhang, Z. Xu, J. Denlinger, A. Fedorov, H. Yang, W. Duan, H. Yao, Y. Wu, S. Fan, H. Zhang, X. Chen, and S. Zhou, Experimental observation of topological fermi arcs in type-II Weyl semimetal mote2, *Nat. Phys.* **12**, 1105 (2016).
- [72] D. Takane, Z. Wang, S. Souma, K. Nakayama, T. Nakamura, H. Oinuma, Y. Nakata, H. Iwasawa, C. Cacho, T. Kim, K. Horiba, H. Kumigashira, T. Takahashi, Y. Ando, and T. Sato, Observation of Chiral Fermions with a Large Topological Charge and Associated Fermi-Arc Surface States in CoSi, *Phys. Rev. Lett.* **122**, 076402 (2019).
- [73] X.-P. Li, K. Deng, B. Fu, Y. K. Li, D.-S. Ma, J. F. Han, J. Zhou, S. Zhou, and Y. Yao, Type-Iii Weyl semimetals: (TaSe<sub>4</sub>)<sub>2</sub>I, *Phys. Rev. B* **103**, L081402 (2021).